Chapter 17

Performance Analysis of SISO and MIMO FSO Communication Systems Over Turbulent Channels

Kostas Peppas, Hector E. Nistazakis, Vasiliki D. Assimakopoulos and George S. Tombras

Additional information is available at the end of the chapter

http://dx.doi.org/10.5772/48231

1. Introduction

Free-space optical (FSO) communications using intensity modulation and direct detection (IM/DD), is a cost-effective and high bandwidth access technique, which has recently received significant attention and commercial interest for a variety of applications [30, 44]. Optical wireless communication systems are rapidly gaining popularity as effective means of transferring data at high rates over short distances due to the necessity of a cost-effective, license-free, and high-bandwidth access communication technique [12, 30, 36, 44]. These systems facilitate rapidly deployable, lightweight, high-capacity communication without licensing fees and tariffs. Terrestrial FSO is not free of challenges though. A major impairment over FSO links is the atmospheric turbulence, caused by the variations in the refractive index because of inhomogeneities in temperature and pressure changes. In clear weather conditions, the atmospheric turbulence results in fluctuations at the intensity of the received signal, i.e., signal fading, also known as scintillation in optical communication terminology [6, 11]. Turbulence is caused by inhomogeneities of both temperature and pressure in the atmosphere and can severely degrade the link performance, particularly over link distances of 1 km or longer. The performance of this technology depends strongly on the atmospheric conditions between the transmitter and the receiver and the parameters of the link such as the length and the operation wavelength. Effects of fog, rain, atmospheric gases, and aerosols also result in beam attenuation due to photon absorption and scattering [25].

The performance of FSO systems over turbulence channels has been addressed in many previous works. Representative examples can be found in [47, 66, 70, 81] and the references therein. The results presented in these papers have demonstrated that the performance of single-input single-output (SISO) FSO links is severely degraded from turbulence. More specifically, the average bit error probability of such systems is far away from satisfying the typical targets for FSO applications within practical ranges of signal-to-noise ratio. To circumvent this problem, powerful fading mitigation techniques have to be deployed. In the open technical literature on FSO communication, the two most popular existing techniques

for mitigation of the degrading effects of atmospheric turbulence are error control coding in conjunction with interleaving [70], [83] and maximum likelihood sequence detection (MLSD) [82]. However, for most scenarios the first one requires large-size interleavers to achieve the promised coding gains. On the other hand, MLSD requires complicated multidimensional integrations and suffers from excessive computational complexity. Some sub-optimal temporal-domain fading mitigation techniques are further explored in [83] and [84].

Another promising solution is the use of diversity techniques and the most popular scheme is the spatial diversity, i.e., the employment of multiple transmit/receive apertures, a well known diversity technique in Radio-Frequency (RF) systems [46, 48, 49, 61, 69, 72, 78, 80]. By using multiple apertures at the transmitter and/or the receiver, the inherent redundancy of spatial diversity has the potential to significantly enhance the performance. Moreover, the possibility for temporal blockage of the laser beams by obstructions is further reduced and longer distances can be covered through heavier weather conditions [46]. Concerning the performance analysis of FSO systems employing spatial diversity, the technical literature is rather rich. Representative past examples can be found in [14, 19, 21, 26, 27, 29, 46, 54–56, 62, 63, 69, 73–75].

On the other hand, various statistical models, e.g. the log normal, the gamma gamma (G − G), the I-K, the K, the negative exponential, and the Rician log normal distribution, have been used in order to describe the optical channel characteristics with respect to the atmospheric turbulence strength [4, 9, 10, 12, 23, 30, 32, 35, 38, 44, 47, 51–53, 59, 65, 71]. Recently, Al-Habash et al. proposed the G-G distribution [4] as a tractable mathematical model for atmospheric turbulence. This model is a two parameter distribution which is based on a doubly stochastic theory of scintillation and assumes that small-scale irradiance fluctuations are modulated by large-scale irradiance fluctuations of the propagating wave, both governed by independent gamma distributions. This distribution has become the dominant fading channel model for FSO links due to its excellent agreement with measurement data for a wide range of turbulence conditions [4].

For many practical FSO applications, however, irradiance is temporally correlated. Thus the derivation of a correlated G − G model is of significant theoretical and practical interest. It is noted that multivariate distributions have recently attracted the interest within the research community due to their importance in studying the performance of diversity systems operating over a multipath fading channels, see, e.g., [1, 2, 5, 15, 33, 45, 49, 58, 64, 68] and references therein. These distributions are particularly useful in the performance analysis of practical systems configurations where antenna branches are closely spaced and the correlation between diversity signals cannot be ignored [68, Chapt. 9]. In the past, several spatial correlation models have been proposed [5, 68] and used for the performance evaluation of wireless communication systems over correlated fading channels. Among them, the exponential correlation model has gained particular interest [2, 33, 45, 64]. This model corresponds to the scenario of multichannel reception by equispaced diversity antennas, in which the correlation between pairs of combined signals decays as the spacing between antenna branches increases [68].

In this chapter, we investigate the performance of multiple-input-multiple output (MIMO) FSO links over both independent and identically distributed (i.i.d.) G − G turbulence channels as well as for exponentially correlated G − G turbulent channels. A closed-form expression

for the average bit error probability (ABEP) of SISO links is first derived. This result serves as benchmark for the performance analysis of FSO links employing multiple apertures and IM/DD. Rapidly convergent infinite series representations for the joint G − G probability density function (PDF), cumulative distribution function (CDF), and moment generating function (MGF) with exponential correlation are also derived. Based on these statistical results, the outage probability (OP) of selection diversity (SD) receivers as well as the ABEP of single-input-multiple-output (SIMO) FSO systems over exponentially correlated turbulent channels is investigated. Finally, we propose a simple yet highly accurate closed form approximation to the sum of arbitrary i.i.d. G − G variates. In the context of this chapter, the α-μ distribution [79] has been chosen as the convenient approximation, for which the parameters are adequately estimated from the sum of the G − G variates. Based on this result, simple accurate approximations for the OP and ABEP of MIMO FSO systems operating over i.i.d. G − G channels and employing equal gain combining (EGC) at the receiver are provided. Various numerically evaluated and computer simulation results demonstrate the accuracy of the proposed analysis. The validity of the presented analysis is testified by comparing numerically evaluated with equivalent computer simulations performance results.

2. Atmospheric turbulence

The refractive index of the atmosphere in the area between the transmitter and the receiver of a wireless optical link fluctuates randomly due to the atmospheric turbulence [12]. These fluctuations are induced mainly due to temperature oscillations among the atmosphere, the ground and the oceans [8, 12, 13, 24, 39]. More specifically atmospheric turbulence is a phenomenon belonging to different spatial and temporal scales. In the Planetary Boundary Layer (PBL), where human activities take place, it is generated by the wind's interaction with the earth's surface, which is said to be in a state of turbulent motion [18, 20, 37, 76, 77].

Turbulence is responsible for the transfer of heat, matter, and momentum within the PBL. However, it is random in nature and remains a complicated phenomenon with many unsolved aspects. The scientific community relies on the combination of experiments, theory, and computer models to understand it. Turbulence is created by thermal convection, wind shear and by the wind flowing over ground obstacles. Within the PBL, turbulence has a diurnal variation reaching a maximum about midday when the solar radiation is at a maximum. Solar radiation heats the surface which, in turn radiates heat to the air above it that becomes warmer and more buoyant and rises while cooler, denser air descends to displace it. The resulting vertical movement of air, together with flow disturbances around surface obstacles, makes low-level winds extremely irregular thus turbulent. The turbulence intensity depends primarily on the temperature lapse rate, i.e. $\lambda = dT/dH$, which is essentially the rate of temperature increase or decrease with increasing height. Under unstable conditions the temperature decreases with height and a hypothetical parcel of air which is warmer than its surrounding air would tend to rise [18, 20, 37, 76, 77].

Turbulence in the atmosphere is carried by rotational-like motions called eddies, which exist in different length scales characterized by different velocity and time scales. The larger eddies are unstable and break up into smaller ones with the subsequent transfer of the kinetic energy of the initial large eddy. The smaller eddies in turn break up into even smaller eddies and the energy is passed on to the new smaller ones. The energy is passed down from the larger scales to the smaller ones until the viscosity of the fluid (in this case air) can dissipate the

kinetic energy into internal energy (or thermal energy). This is called the energy cascade and it is one of the main characteristics of turbulent motion. Other important features of turbulence are irregularity (or chaotic), diffusivity (mixing), turbulent diffusion (molecular diffusivity), rotationality (always three dimensional, the mechanism that aids the energy cascade), dissipation (the transfer of energy from larger to smaller eddies), length scales of turbulent eddies. The size of eddies spans from the order of a few millimetres to meters, namely the inner and outer scales, respectively [18, 20, 37, 76, 77]. This inner and outer scales is the main phenomenon for the choice of the appropriate distribution for turbulence's mathematical representation.

It is commonly known that in turbulent flow the actual flow velocity is broken into the mean velocity $\vec{U}$ plus the fluctuating turbulent velocity component $\vec{u}$, in the three directions, respectively. Thus, in the x-axis the instantaneous flow velocity is $U_x + u_x$. The values of the turbulent components namely u_x, u_y and u_z may not be expressed as functions of time, but a statistical description is only possible. Turbulence within the PBL can degrade the performance of free-space optical links, particularly over ranges of the order of 1 km or longer. This phenomenon is not caused by the turbulent eddies which possess different velocities but only by the parcels of air with different temperatures (and thus different densities) rising or descending that cross the path of the FSO links. They cause inhomogeneities in the temperature and pressure profiles of the atmosphere and lead to variations of the refractive index along the transmission path. Based on the fluctuations of the air density, the scientific community has developed the refractive index structure parameter C_n^2 (related to the temperature structure one, i.e. C_T^2) which takes different values depending on the strength of turbulence. The parameter C_n^2 may be measured experimentally of computed theoretically if one knows the outer scale of turbulence (i.e., the large eddy size scale) and the potential refractive index [18, 20, 37, 76, 77]. Additionally, as we will demonstrate below, there are many mathematical models for the estimation of the C_n^2 value [6, 7, 44, 52]

Thus, these variation of the refraction index in the free space area that the beam of the optical link propagates and causes deflections of the light beam into and mostly out of the transmit path [17, 52]. This random radiation of the laser beam results in fluctuations of the optical signal's irradiance at the receiver's side. This phenomenon is the so-called scintillation [4, 12, 17, 31, 42–44, 51]. The influence of scintillation in the performance of the wireless optical communication systems is very strong for the terrestrial links because induces fading of the signal arriving at the receiver in a random way. Thus, in order to estimate the optical signal arriving at the receiver it is necessary to study the appropriate statistical distribution which describes the fading statistics of each area.

Many statistical models have been proposed for the simulation of these fading statistics caused by the atmospheric turbulence effect. Some of them have been arising from experimental results, while, others, from theoretical studies. It is obvious that each location has irregularities, depending on the ground's morphology, the weather conditions, the time of the day [7, 24] and the turbulence strength. The proposed statistical models concern weak, moderate, strong or very strong turbulence conditions and the turbulence strength can be estimated through the turbulence parameter C_n^2, which depends on many parameters of the weather conditions.

One of the statistical parameters that we are using for the practical estimation of scintillation's influence at the wireless optical links' performance,is the scintillation index which is given by

the following mathematical expression [44]:

$$\sigma_I^2 = \frac{< I^2 > - < I >^2}{< I >^2} \tag{1}$$

with I being the optical signal's irradiance at the receiver and $<>$ represents the ensemble average value. In the weak scintillation theory, under the assumption of plane wave propagation, the scintillation index is proportional to the Rytov variance and is given as [44]:

$$\sigma_{I,R}^2 = 1.23 C_n^2 k^{7/6} L^{11/6} \tag{2}$$

where C_n^2 is the parameter of turbulence, $k = 2\pi/\lambda$ is the optical wavenumber, while L is the link's length [44, 49, 52].

If we assume spherical wave propagation, $\sigma_{I,R}$ can be expressed as [44]:

$$\sigma_{I,R}^2 = 0.5 C_n^2 k^{7/6} L^{11/6} \tag{3}$$

In order to estimate the influence of the atmospheric turbulence conditions in the wireless optical communication system's performance, we assume a horizontal propagation path of up to a few kilometers (usually the FSO link is smaller than 4-5 km), where the turbulence strength value is considered as constant [50, 52]. Many models has been proposed for the estimation of the turbulence parameter C_n^2 [6, 12, 34, 44]. The most widely employed in research literature, are the so-called Hufnagel-Valley model and the Hufnagel and Stanley model, the SLC Day model and the SLC Night model [6, 7, 12, 34, 44, 49, 52].

The estimation of the parameter C_n^2 through the Hufnagel-Valley model (or HV5/7 model) [7, 44], depends on the wind speed, v, and the altitude, h, where the wireless optical link operates. The values 5 and 7 of the abbreviation of the Hufnagel-Valley model (i.e. HV5/7) correspond to the atmospheric coherence length (r_0) in cm and the isoplantic angle (θ_0) in μrad respectively, for $\lambda = 0.55\mu m$ while for $\lambda = 1.315\mu m$ the above values are 14cm and 20 μrad respectively [7, 44, 52]. The mathematical expression of the HV5/7 is the following [7, 44, 51],

$$C_n^2(h) = 0.00594(u/27)^2 (10^{-5}h)^{10} e^{h/1000} + 2.7 \times 10^{-6} e^{-h/1500} + C_n^2(0) e^{-h/1000} \tag{4}$$

where $C_n^2(0)$ is the value of C_n^2 at the sea level in $m^{-2/3}$. In general, the turbulence parameter C_n^2 varies between the values 10^{-17} $m^{-2/3}$ and 10^{-13} $m^{-2/3}$ for weak up to very strong turbulence cases, respectively, [44, 51].

Another significant model for the estimation of the turbulence parameter is proposed by Hufnagel and Stanley [12, 34, 52]. Its mathematical expression is the following,

$$C_n^2(h) = K_0 h^{-1/3} e^{-h/h_0} \tag{5}$$

with K_0 being the turbulence strength parameter and depends on the characteristics of the specific location where the wireless optical link has been installed and h is the altitude.

Another model for the estimation of the atmospheric turbulence parameter, C_n^2, is the SLC Day model which depends only on the height where the FSO link operates [7, 52]. The

mathematical expression for this model, which is accurate enough for daytime hours, is given as:

$$C_n^2(h) = \begin{cases} 1.7 \times 10^{-14} & \text{if } 0 < h < 18.5\text{m}; \\ \frac{3.13 \times 10^{-13}}{h^{1.05}} & \text{if } 18.5 < h < 240\text{m}; \\ 1.3 \times 10^{-15} & \text{if } 240 < h < 880\text{m}; \\ \frac{8.87 \times 10^{-7}}{h^3} & \text{if } 880 < h < 7200\text{m}; \\ \frac{2.0 \times 10^{-16}}{h^{0.5}} & \text{if } 7200 < h < 20000\text{m}; . \end{cases} \tag{6}$$

while for accurate results for night hours are given by the SLC Night model [7, 52], depends only on the height where the optical link operates like the previous model are given by the following expression:

$$C_n^2(h) = \begin{cases} 8.4 \times 10^{-15} & \text{if } 0 < h < 18.5\text{m}; \\ \frac{2.87 \times 10^{-12}}{h^2} & \text{if } 18.5 < h < 110\text{m}; \\ 2.5 \times 10^{-16} & \text{if } 110 < h < 1500\text{m}; \\ \frac{8.87 \times 10^{-7}}{h^3} & \text{if } 1500 < h < 7200\text{m}; \\ \frac{2.0 \times 10^{-16}}{h^{0.5}} & \text{if } 7200 < h < 20000\text{m}; . \end{cases} \tag{7}$$

The above mentioned models for the estimation of the turbulence parameter C_n^2, (i.e HV5/7, Hufnagel and Stanley, SLC Day and SLC Night), are valid mainly for wireless optical links which have been installed over terrestrial area. Thus, the estimation of the turbulence parameter for paths over maritime area can be done through the following accurate approximation which is valid for low altitude and for specific constant parameters c_1, c_2, c_3, c_4 and c_5. The values of the constant parameters are given in [41, 44] and the corresponding mathematical form is the following:

$$C_n^2(h) = c_1 + c_2 e^{-h/c_3} + c_4 e^{-h/c_5} \tag{8}$$

Obviously, as we mentioned above, for the estimation of the turbulence strength through the above Equations, we assumed that the value of C_n^2 remains constant for relatively long time interval and for the whole, horizontal, propagation path. This assumption is not always very accurate and thus, in some cases, it is necessary to handle this parameter as a random variable (RV), which follows a specific distribution [35, 52].

3. The Gamma-Gamma wireless optical channel model revisited

In the G − G channel model for atmospheric turbulence channels the PDF of the irradiance I can be derived from the product of two independent Gamma-distributed RVs x and y with suitably defined parameters [4]. The PDF of the G − G distribution is given by [44]

$$f_I(I) = \frac{2(km)^{(k+m)/2}}{\Gamma(k)\Gamma(m)\overline{I}} \left(\frac{I}{\overline{I}}\right)^{\frac{k+m}{2}-1} K_{k-m}\left[2\sqrt{km\left(\frac{I}{\overline{I}}\right)}\right] \tag{9}$$

where $K_\alpha(\cdot)$ is the modified Bessel function of the second kind and order α, $\Gamma(\cdot)$ is the gamma function and $\mathbb{E}\langle I\rangle$ with $\mathbb{E}\langle\cdot\rangle$. denoting expectation. The parameters $k > 0$ and $m > 0$ can be properly adjusted to provide good agreement between theoretical and experimental data.

Assuming spherical wave propagation, k, m can be directly related to atmospheric conditions through the following expressions [14]

$$k = \left[\exp\left(\frac{0.49\sigma_{I,R}^2}{\left(1 + 0.18d^2 + 0.56\sigma_{I,R}^{12/5}\right)^{7/6}} \right) - 1 \right]^{-1} \tag{10}$$

$$m = \left[\exp\left(\frac{0.51\sigma_{I,R}^2 \left(1 + 0.69\sigma_{I,R}^{12/5}\right)^{-5/6}}{1 + 0.90d^2 + 0.62d^2\sigma_{I,R}^{12/5}} \right) - 1 \right]^{-1} \tag{11}$$

where $\sigma_{I,R}$ is the Rytov variance defined above and $d = \sqrt{kD^2/4L}$, with D being the aperture diameter of the receiver.

The corresponding CDF can be expressed as [21]

$$F_I(I) = \frac{1}{\Gamma(k)\,\Gamma(m)}\, G_{1,3}^{2,1}\left[\frac{km}{\overline{I}}\, I \,\Big|_{k,\,m,\,0}^{1} \right] \tag{12}$$

with $G_{p,q}^{m,n}[\cdot]$ being the Meijer-G function [60, Eq. (8.2.1.1)] [1].

The $\nu-$th moment of I defined as $\mathbb{E}\{X^\nu\} = \int_0^\infty f_I(I)\mathrm{d}I$ can be obtained using [28, Eq. (6.561/16)] as

$$\mathbb{E}\{I^\nu\} = \left(\frac{k\,m}{\overline{I}}\right)^{-\nu} \frac{\Gamma(k+\nu)\Gamma(m+\nu)}{\Gamma(k)\Gamma(m)} \tag{13}$$

For the correlated test case, to obtain an analytical expression for the multivariate G-G distribution, we first define $\mathbf{N}$ independent Gamma-distributed RVs W_n, $n = 1, 2, \ldots, \mathbf{N}$, with marginal PDFs given by [70, Eq. (2)]

$$f_{W_n}(w_n) = \frac{k^k\, w_n^{k-1}}{\Gamma(k)} \exp\left(-k\, w_n\right)\, H\left(w_n\right) \tag{14}$$

where $k \geq 1/2$ is the distribution's shaping parameter and $H(\cdot)$ the unit step function [28, p. xliv]. Also, let Y_n's be correlated Gamma-distributed RVs with correlation matrix given by $\mathbf{\Sigma}_{i,j} = \rho^{|i-j|}$, where $0 \leq \rho < 1$ is the power correlation coefficient [68, Eq. (9.195)]. Performing $\mathbf{N}$ RVs transformations in [33, Eq. (3)] and using [28, Eq. (8.445)], the joint PDF of $\mathbf{Y} = [Y_1\, Y_2\, \cdots\, Y_{\mathbf{N}}]$ is obtained as

$$\begin{aligned} f_{\mathbf{Y}}(\mathbf{y}) =& \frac{\left(1-\rho^2\right)^m}{\Gamma(m)} \exp\left[-\frac{m}{\overline{u}\,(1-\rho^2)}\,(y_1 + y_{\mathbf{N}}) - \frac{m\,\left(1+\rho^2\right)}{\overline{u}\,(1-\rho^2)} \sum_{j=2}^{\mathbf{N}-1} y_j \right] \\ &\times \sum_{i_1, i_2, \ldots, i_{\mathbf{N}-1}=0}^{\infty} \left[\frac{m}{\overline{u}\,(1-\rho^2)} \right]^{\mathbf{N}m + 2\sum_{j=1}^{\mathbf{N}-1} i_j} y_1^{q_1-1}\, y_{\mathbf{N}}^{q_{\mathbf{N}}-1} \prod_{j=2}^{\mathbf{N}-1} y_j^{q_j-1} \prod_{n=1}^{\mathbf{N}-1} \left[\frac{1}{\Gamma\left(m+i_n\right)\, i_n!} \right] \end{aligned} \tag{15}$$

[1] The Meijer-G function is a standard built-in function available in the most popular mathematical software packages, such as Maple or Mathematica

where $\mathbf{y} = [y_1\, y_2\, \cdots\, y_{\mathbf{N}}]$, with $y_n > 0, \forall\, n$, $m \geq 1/2$ is the distribution's shaping parameter, and

$$q_j = \begin{cases} m + i_1 & \text{if } j = 1; \\ m + i_{\mathbf{N}-1} & \text{if } j = \mathbf{N}; \\ m + i_{j-1} + i_j & \text{if } j = 2, 3, \ldots, \mathbf{N} - 1. \end{cases} \tag{16}$$

Then, following the approach presented in [70] and [40], the multivariate G-G distribution with exponential correlation can be derived as [70, Eq. (5)]

$$f_{\mathbf{I}}(\mathbf{I}) = \int_0^{\infty} \int_0^{\infty} \cdots \int_0^{\infty} \prod_{n=1}^{\mathbf{N}} \left[y_n^{-1} f_{W_n}\left(\frac{I_n}{y_n}\right)\right] f_{\mathbf{Y}}(\mathbf{y})\, \mathrm{d}\mathbf{y} \tag{17}$$

where $\mathbf{I} = [I_1\, I_2\, \cdots\, I_{\mathbf{N}}]$, with $I_n = W_n\, Y_n, \forall\, n$, Substituting (14) and (15) to (17) and using [28, Eq. (3.471/9)], the joint PDF of $\mathbf{I}$ is obtained as

$$\begin{aligned} f_{\mathbf{I}}(\mathbf{I}) =& \frac{2^{\mathbf{N}}\left(1-\rho^2\right)^m}{[\Gamma(k)]^{\mathbf{N}}\,\Gamma(m)} \sum_{i_1, i_2, \ldots, i_{\mathbf{N}-1}=0}^{\infty} \Xi^{\frac{\mathbf{N}(k+m)}{2} + \sum_{j=1}^{\mathbf{N}-1} i_j} \rho^{2\sum_{j=1}^{\mathbf{N}-1} i_j} \\ & \times I_1^{\omega_1} K_{q_1-k}\left[2\sqrt{\Xi\, I_1}\right] u_{\mathbf{N}}^{\omega_{\mathbf{N}}} K_{q_{\mathbf{N}}-k}\left[2\sqrt{\Xi\, I_{\mathbf{N}}}\right] \\ & \times \prod_{j=2}^{\mathbf{N}-1} \left\{ \frac{I_j^{\omega_j}}{\left(1+\rho^2\right)^{\frac{q_j-k}{2}}} K_{q_j-k}\left[2\sqrt{\Xi\left(1+\rho^2\right) I_j}\right]\right\} \prod_{n=1}^{\mathbf{N}-1} \left[\frac{1}{\Gamma(m+i_n)\, i_n!}\right] \end{aligned} \tag{18}$$

with $\Xi = (k\, m)/[\overline{I}\,(1-\rho^2)]$, $\omega_n = (k+q_n)/2 - 1, \forall\, n = 1, 2, \ldots, \mathbf{N}$. Note that for $\rho = 0$, all infinite series terms that appear in (18) with $i_j \neq 0, \forall\, j$, vanish and (18) simplifies to the product of $\mathbf{N}$ independent G-G distributions [16, Eq. (2)].

Next, important statistical properties of the exponentially correlated multivariate G-G distribution, namely the joint G-G CDF and MGF will be presented.

3.1. Joint CDF

The joint CDF of $\mathbf{I}$ is given by

$$F_{\mathbf{I}}(\mathbf{I}) = \int_0^{I_1} \int_0^{I_2} \cdots \int_0^{I_{\mathbf{N}}} f_{\mathbf{I}}(\mathbf{t})\, \mathrm{d}\mathbf{t} \tag{19}$$

with $\mathbf{t} = [t_1\, t_2\, \cdots\, t_{\mathbf{N}}]$. In order to obtain an analytical expression for (19), the Bessel functions that appear in (18) are expressed in terms of Meijer-G functions [60, Eq. (8.4.3.1)]. Then, using [60, Eq. (8.4.23.1)], [60, Eq. (2.24.1.1)], and [60, Eq. (8.2.2.15)], an analytical expression for the joint G-G CDF with exponential correlation is derived in infinite series form as

$$\begin{aligned} F_{\mathbf{I}}(\mathbf{I}) =& \frac{\left(1-\rho^2\right)^m}{[\Gamma(k)]^{\mathbf{N}}\,\Gamma(m)} \sum_{i_1, i_2, \ldots, i_{\mathbf{N}-1}=0}^{\infty} \prod_{n=1}^{\mathbf{N}-1} \left[\frac{\rho^{2i_n}}{\Gamma(m+i_n)\, i_n!}\right] \mathcal{G}(q_1,\, k,\, \Xi\, I_1) \\ & \times \mathcal{G}(q_{\mathbf{N}},\, k,\, \Xi\, I_{\mathbf{N}}) \prod_{j=2}^{\mathbf{N}-1} \left\{ \mathcal{G}\left[q_j, k, \Xi\left(1+\rho^2\right) I_j\right] \left(1+\rho^2\right)^{-q_j}\right\} \end{aligned} \tag{20}$$

where

$$\mathcal{G}(A, B, x) = G_{1,3}^{2,1}\left[x \,\middle|\, \begin{matrix} 1 \\ A, B, 0 \end{matrix}\right]. \tag{21}$$

3.2. Joint MGF

Using $f_{\mathbf{I}}(\mathbf{I})$, the joint MGF of $\mathbf{I}$ can be obtained as

$$\mathcal{M}_{\mathbf{I}}(\mathbf{s}) = \int_0^\infty \int_0^\infty \cdots \int_0^\infty \exp\left(-\sum_{n=1}^{\mathbf{N}} s_n I_n\right) f_{\mathbf{I}}(\mathbf{I})\, \mathrm{d}\mathbf{I} \tag{22}$$

with $\mathbf{s} = [s_1\, s_2\, \cdots\, s_{\mathbf{N}}]$. Substituting (18) in (22) and using [60, Eq. (8.4.3.1)], [60, Eq. (8.4.23.1)], [60, Eq. (2.24.1.1)], and [60, Eq. (8.2.2.15)], an analytical expression for the joint G-G MGF is derived as

$$\begin{aligned}\mathcal{M}_{\mathbf{I}}(\mathbf{s}) =& \frac{(1-\rho^2)^m}{[\Gamma(k)]^{\mathbf{N}}\,\Gamma(m)} \sum_{i_1,i_2,\ldots,i_{\mathbf{N}-1}=0}^{\infty} \prod_{j=1}^{\mathbf{N}-1} \left[\frac{\rho^{2i_j}}{\Gamma\left(m+i_j\right)\, i_j!}\right] \mathcal{H}\left(q_1, k, \frac{\Xi}{s_1}\right) \\ &\times \mathcal{H}\left(q_{\mathbf{N}}, k, \frac{\Xi}{s_{\mathbf{N}}}\right) \prod_{j=2}^{\mathbf{N}-1} \left\{\mathcal{H}\left[q_j, k, \frac{\Xi\left(1+\rho^2\right)}{s_j}\right] \left(1+\rho^2\right)^{-q_j}\right\}\end{aligned} \tag{23}$$

where

$$\mathcal{H}(A, B, x) = G_{1,2}^{2,1}\left[x \,\middle|\, \begin{matrix} 1 \\ A, B \end{matrix}\right]. \tag{24}$$

4. System model

We consider a MIMO FSO system where the information signal is transmitted via M apertures and received by N apertures. The information bits are modulated using IM/DD with on-off keying (OOK) and transmitted through the M apertures using repetition coding [14]. A high-energy FSO system whose performance is limited by background radiation and thermal noise is assumed. Under this assumption, the use of the AWGN model as a good approximation of the Poisson photon counting detection model is applicable [46]. The received signal at the n-th receive aperture is expressed as

$$r_n = \eta s \sum_{m=1}^{M} I_{mn} + v_n,\ n = 1, \ldots, N \tag{12}$$

where η is the optical-to-electrical conversion coefficient, $s \in \{0, 1\}$ represents the information bits and v_n is the AWGN with zero mean and variance $\sigma_v^2 = N_0/2$. In the following analysis, we assume that the I_{mn}-s are either independent or exponentially correlated G-G random variables. It is noted that the assumption of independence can significantly simplify the underlying mathematical analysis and it is justified for link distances of the order of kilometers and for aperture separation distances of the order of centimeters [14]. Finally, we define the instantaneous electrical signal-to-noise ratio (SNR) as $\mu_{mn} \triangleq (\eta I_{mn})^2/N_0$ and the corresponding average electrical SNR as $\overline{\mu}_{mn} \triangleq (\eta \mathbb{E}\langle I_{mn}\rangle)^2/N_0$.

5. Performance analysis of SISO links

The ABEP of the considered system in the presence of AWGN and under the assumption of perfect channel state information (CSI) at the receiver side is given by

$$P_e = P(1)P(e|1) + P(0)P(e|0) \tag{13}$$

where $P(1)$ and $P(0)$ are the probabilities of sending 1 and 0 bits, respectively, and $P(e|1)$, $P(e|0)$ are the conditional bit-error probabilities bit 1 or 0 has been transmitted, respectively. Without loss of generality, we assume $P(1) = P(0) = 0.5$ and $P(e|1) = P(e|0)$, a fact also justified by the symmetry of the problem. Using the analysis presented in [46] one obtains

$$P(e|I) = P(e|1, I) = P(e|0, I) = Q\left(\frac{\eta I}{\sqrt{2N_0}}\right) \tag{14}$$

where $Q(x) = \frac{1}{\sqrt{2\pi}} \int_x^\infty \exp\left(-\frac{t^2}{2}\right) \mathrm{d}t$ is the Gauss-Q function. The ABEP can be obtaining by averaging $P(e|I)$ over the PDF of I, namely

$$\overline{P}_{be} = \int_0^\infty P(e|I) f_I(I) \mathrm{d}I \tag{15}$$

By expressing $P(e|I)$ in terms of the electrical SNR μ, namely $Q\left(\frac{\eta I}{\sqrt{2N_0}}\right) = Q\left(\sqrt{\frac{\mu}{2}}\right) = 0.5\mathrm{erfc}\left(\frac{\sqrt{\mu}}{2}\right)$, $\overline{P}_{be}$ can be obtained by performing a change of variables and averaging over the PDF of the electrical SNR, μ, instead of the PDF of I. Assuming that I follows a $\mathrm{G}-\mathrm{G}$ distribution with parameters k and m and by applying a simple power transformation of RVs, the PDF of μ can be expressed as

$$f_\mu(\mu) = \frac{(km)^{(k+m)/2}}{\Gamma(k)\Gamma(m)\sqrt{\overline{\mu}\mu}} \left(\sqrt{\frac{\mu}{\overline{\mu}}}\right)^{\frac{k+m}{2}-1} K_{k-m}\left[2\sqrt{km\sqrt{\frac{\mu}{\overline{\mu}}}}\right] \tag{16}$$

Finally $\overline{P}_{be}$ can be expressed in closed form as

$$\overline{P}_{be} = 0.5\mathcal{F}\left(k, m, \overline{\mu}, \frac{1}{2}\right) \tag{17}$$

where $\mathcal{F}(k, m, \overline{\mu}, s)$ is given by [57, Eq. (27)] [2]

$$\mathcal{F}(k, m, \overline{\mu}, s) = \frac{\Xi^{k+m} s^{-(k+m)/2}}{4\pi^{\frac{3}{2}}\Gamma(k)\Gamma(m)} G_{2,5}^{4,2}\left[\frac{k^2 m^2}{16\overline{\mu}s^2}\middle|\begin{matrix}a_p\\ b_q\end{matrix}\right] \tag{16}$$

with $a_p = \{1 - \frac{k+m}{4}, \frac{1}{2} - \frac{k+m}{4}\}$, $b_q = \{\frac{1}{2} + \frac{k-m}{4}, \frac{k-m}{4}, \frac{1}{2} + \frac{m-k}{4}, \frac{m-k}{4}, -\frac{k+m}{4}\}$ and $\Xi \triangleq \sqrt{\frac{km}{\sqrt{\overline{\mu}}}}$.

Another important performance metric is the outage probability. The outage probability is defined as the probability that the SNR of the signal at the output of the receiver, μ , falls below a specified threshold, μ_{th}. This metric is considered as an important parameter for FSO links to be operated as a part of a data network and is critical in the design of both transport and network layer [21]. With the help of (12) and assuming $\overline{I} = 1$, the outage probability is obtained in closed form as

$$P_{\mathrm{out}} = \Pr\{\mu < \mu_{\mathrm{th}}\} = \Pr\left\{\frac{I^2\eta^2}{N_0} < \mu_{\mathrm{th}}\right\} = \Pr\left\{I < \sqrt{\frac{\mu_{\mathrm{th}}}{\overline{\mu}}}\right\} = F_I\left(\sqrt{\frac{\mu_{\mathrm{th}}}{\overline{\mu}}}\right) \tag{17}$$

[2] It is noted that Eq. (27) in [57] includes typos which we have corrected in (16)

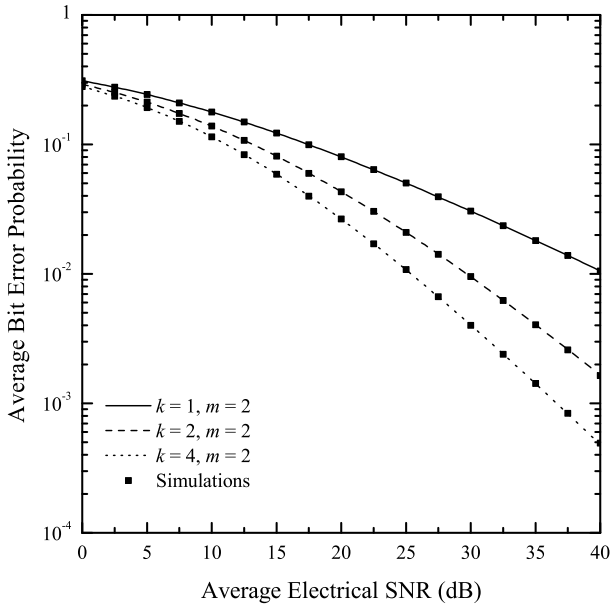

Figure 1. Average Bit Error Probability of SISO OOK receivers employing intensity modulation and direct detection and operating over G − G channels, for different values of parameters k and m, as a function of the Average Electrical SNR, $\overline{\mu}$.

Using (16), in Figure 1 the ABEP of SISO OOK receivers employing intensity modulation and direct detection and operating over G − G channels is depicted, for different values of parameters k and m, as a function of the Average Electrical SNR, $\overline{\mu}$. Moreover, in Figure 2 the OP of the system under consideration is depicted for the same set of parameters as a function of the inverse normalized outage threshold, $\frac{\mu_{\text{th}}}{\overline{\mu}}$.

As it can be observed, for a SISO FSO link, both the ABEP and OP performance is quite poor (i.e., higher than 10^{-3} in the SNR range of 30-40 dB , especially over strong atmospheric turbulence conditions (that corresponds to small values of k or m) and therefore the use of diversity techniques is absolutely justified. The use of spatial diversity can be implemented either at the transmitter (MISO) or at the receiver (SIMO case) or at both of them (MIMO case). In both figures, our numerically evaluated results are accompanied with semi-analytical Monte Carlo simulations. In our simulations, more than 10^6 square G − G samples are generated to guarantee statistical convergence. The following listings, written in Matlab 2008a demonstrate the evaluation of the ABEP and OP for the SISO case using Monte Carlo simulations.

```
function y = BER_OOK(SNR_dB, k, m, SIZE)
%SNR_dB: average electical SNR
%k, m: the distribution parameters
mu_bar = 10^(0.1*SNR_dB);
% The first gamma process:
g = gamrnd(k, sqrt(mu_bar)/k, 1, SIZE);
% The second gamma process:
```

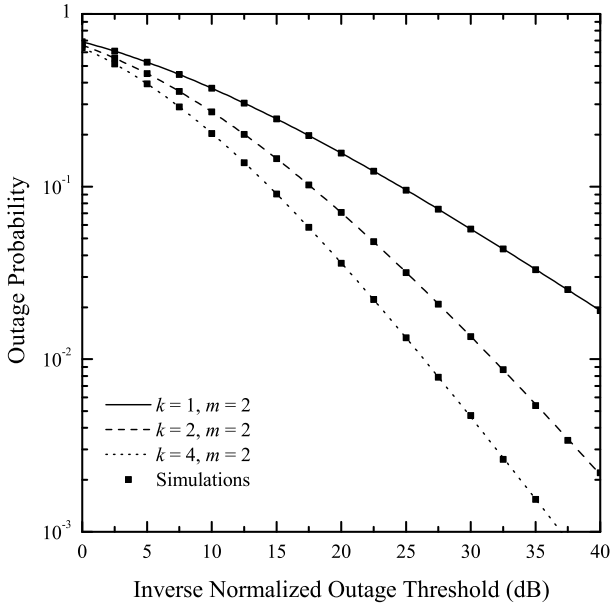

Figure 2. Outage Probability of SISO receivers employing intensity modulation and direct detection and operating over G − G channels, for different values of parameters k and m, as a function of the Inverse Normalized Outage Threshold, $\overline{\mu}/\mu_{th}$.

```
data = gamrnd(m, g/m, 1, SIZE);
% The final data
data = data.^2;
% ABEP of OOK
y = sum( 0.5*erfc(0.5*sqrt(data)))/SIZE;

function y = outage(k, m, inverse_th_dB, SIZE)
th = 10^(0.1*inverse_th_dB);
% first gamma process
first = gamrnd(k, 1/k, 1, SIZE);
% final process
data = (gamrnd(m, first/m, 1, SIZE));
y = length(find(data < 1/sqrt(th)))/SIZE;
```

In the following analysis, analytical results for both SIMO and MIMO cases will be presented.

5.1. SIMO case: Selection Diversity (SD)

The SD combining scheme is the least complicated among the considered combining schemes because of the fact that it processes the aperture with the maximum received irradiance (or electrical SNR). Consequently, the selection is made according to

$$I_{\mathrm{SD}} = \max\{I_1, I_2 \cdots, I_N\} \tag{18}$$

If I_n are i.i.d random variables, then using a similar to the previous section analysis, the OP of SD receivers is readily obtained as

$$P_{\text{out}} = \left[F_I \left(\sqrt{\frac{\mu_{\text{th}}}{\overline{\mu}}} \right) \right]^N \tag{19}$$

If exponentially correlated irradiance is considered, the CDF of I_{SD} is readily obtained using (20) as

$$P_{\text{out}}(\gamma_{\text{th}}) = F_{\mathbf{I}} \left(\sqrt{\frac{\mu_{\text{th}}}{\overline{\mu}}}, \cdots, \sqrt{\frac{\mu_{\text{th}}}{\overline{\mu}}} \right). \tag{20}$$

In Figure 3 the OP of three- and four-branch SIMO receivers employing intensity modulation and direct detection and operating over exponentially correlated G − G channels, for $\rho = 0.25$ and different values of parameters k and m, is depicted as a function of the Inverse Normalized Outage Threshold, $\overline{\mu}/\mu_{th}$. As it can be observed, the employment of spatial diversity significantly enhances the outage performance of the considered system. To double-check the correctness of the proposed analysis, the analytical results are accompanied with numerical ones obtained using Monte-Carlo simulations. Because of the long computational time, inherent to Monte-Carlo methods, simulation results of up to 10^{-6} are given. In order to generate exponentially correlated G − G samples, we make use of the fact that I_n can be written as $I_n = W_n Y_n, \forall n$. where W_n and Y_n are samples of an uncorrelated and a correlated gamma process, respectively. Uncorrelated gamma samples with given parameters can be easily generated using the standard Matlab built-in function $gamrnd()$. The generation of correlated gamma random samples with given correlation matrix has been addressed in several past works. In the context of this work, we used the method presented in [67], which yields accurate results for the given system parameters, despite the fact that it imposes certain conditions or constraints on the PDF parameters. Finally, it is noted that although the analytical expression for the outage probability is given in terms of infinite series, it converges rapidly and steadily, requiring few terms to obtain sufficient numerical accuracy. As it was shown in [56], the number of terms depends on the values of the parameters k and m, the correlation coefficient as well as the SNR. In our terms, a truncation of the infinite series to 25 terms and 18 terms for the three- and four-branch case, respectively, resulted in an excellent match of the numerical results with the Monte-Carlo simulations.

5.2. SIMO case: Optimal combining

When receive diversity with optimal combining (OC) is applied, following a similar analysis as in [46], the ABEP is obtained as

$$\overline{P}_{be} = \int_0^\infty \int_0^\infty \cdots \int_0^\infty f_{\mathbf{I}}(\mathbf{I})\, Q\left(\frac{\eta}{\sqrt{2\, N\, N_0}} \sqrt{\sum_{n=1}^{N} I_n^2} \right) \mathrm{d}\mathbf{I} \tag{21}$$

where the average irradiance is considered to be normalized to one.

In the following analysis, we assume that I_n are exponentially correlated G-G random variables. In general, the N-fold integral in (21) is difficult, if not impossible to be obtained in closed form. To circumvent this problem, we utilize a simple and accurate exponential

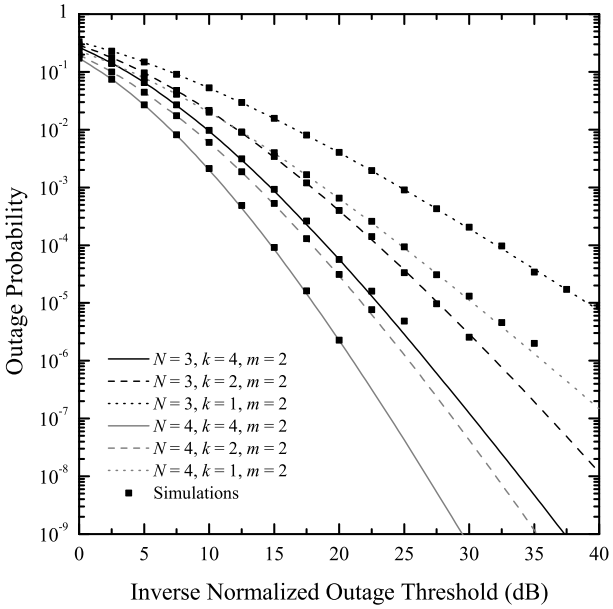

Figure 3. Outage Probability of triple and quadruple branch SIMO receivers employing intensity modulation and direct detection with selection diversity and operating over exponentially correlated G − G channels, for $\rho = 0.25$ and different values of parameters k and m, as a function of the Inverse Normalized Outage Threshold, $\overline{\mu}/\mu_{th}$.

approximation for the Gaussian-Q function using [22, eq. (2)] and [22, eq. (14)] namely

$$Q(x) \cong \frac{1}{12}\exp\left(-\frac{x^2}{2}\right) + \frac{1}{4}\exp\left(-\frac{2\,x^2}{3}\right). \tag{22}$$

Substituting (22) in (21) and using [60, Eq. (8.4.3.1)], [60, Eq. (8.4.23.1)], and [60, Eq. (2.24.1.1)], yields

$$\overline{P}_{be} \cong \frac{1}{12}\mathcal{N}\left(k, m, \sqrt{\frac{\mu}{4\,N}}\right) + \frac{1}{4}\mathcal{N}\left(k, m, \sqrt{\frac{\mu}{3\,N}}\right) \tag{23}$$

where μ is the average electrical SNR and

$$\begin{aligned}\mathcal{N}(k,m,s) =& \frac{2^{N(m+k-2)}\left(1-\rho^2\right)^m}{\pi^N\left[\Gamma(k)\right]^N\Gamma(m)} \sum_{i_1,i_2,..,i_{N-1}=0}^{\infty} (2\rho)^{2\sum_{j=1}^{N-1} i_j} \prod_{n=1}^{N}\left[\frac{1}{\Gamma(m+i_n)\,i_n!}\right] \\ &\times \mathcal{I}(q_1,k,\Xi,s)\,\mathcal{I}(q_N,k,\Xi,s)\prod_{j=2}^{N-1}\left\{\mathcal{I}\left[q_j,k,\Xi\left(1+\rho^2\right),s\right]\left(1+\rho^2\right)^{-q_j}\right\}\end{aligned} \tag{24}$$

with

$$\mathcal{I}(A,B,C,x) = G_{4,1}^{1,4}\left[\frac{16\,x^2}{C^2}\,\middle|\,\begin{matrix}\frac{1-A}{2}, \frac{2-A}{2}, \frac{1-B}{2}, \frac{2-B}{2} \\ 0\end{matrix}\right]. \tag{25}$$

Figure 4 illustrates the ABEP performance of OC FSO links, operating at $\lambda = 1550$nm with $N = 3$ and 4 receive apertures, versus μ. Similarly to [70], exponentially correlated

atmospheric turbulence channels are considered with $\rho = 0.175$. It is assumed that $C_n^2 = 1.7 \times 10^{-14}$, which is a typical value of refractive index for FSO links near the ground during daytime. Furthermore, it is assumed that $D \ll L$ leading to $d = 0$, and hence, no aperture averaging is possible. Three different link distances are considered: $L = 3$, 4, and 5 km. The resulting values for k and m are obtained via (10) and (11), respectively. As expected, the ABEP improves as N and/or μ increase and/or L decreases. Furthermore, as it is shown comparing numerically evaluated results for the ABEP with the equivalent exact ones obtained via Monte Carlo simulations, the proposed ABEP approximation given by (23) provides a tight upper bound for all test cases under consideration.

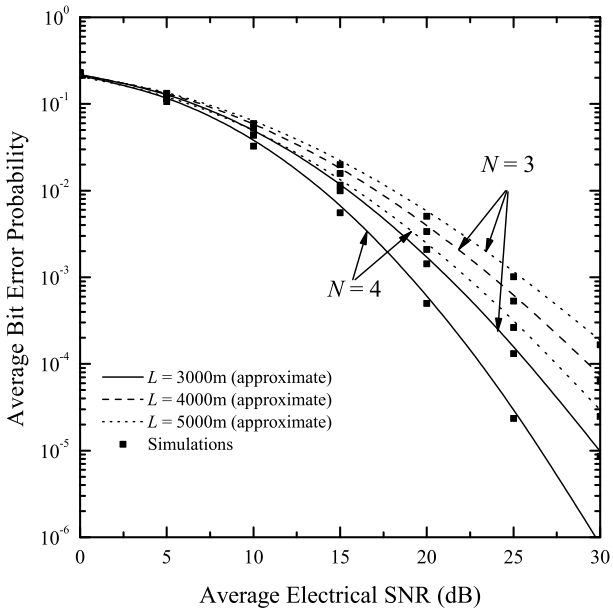

Figure 4. ABEP of triple and quadruple branch SIMO FSO links operating over exponentially correlated G − G atmospheric turbulent channels and employing optimal combining, versus average electrical SNR μ for $\rho = 0.175$ and different link distances.

5.3. MIMO case: Equal gain combining

Assuming perfect Channel State Information (CSI), the ABEP of the considered FSO system is given by [46]

$$\overline{P}_{be} = \int_0^\infty \int_0^\infty \cdots \int_0^\infty f_{\mathbf{I}}(\mathbf{I})\, Q\left(\frac{\eta}{N M \sqrt{2 N_0}} \sum_{n=1}^{N} I_n\right) \mathrm{d}\mathbf{I} \tag{26}$$

which can be further expressed as [21]

$$\overline{P}_{be} = \frac{1}{2} \int_0^\infty f_I(I)\, \mathrm{erfc}\left(\frac{\eta}{2 M N \sqrt{N_0}} I\right) \mathrm{d}I \tag{27}$$

where $I = \sum_{n=1}^{N} I_n$. This integral is very difficult to be obtained in closed form since an analytical expression for the statistical distribution of I is required. In the following it will be shown that when I_n are i.i.d G-G random variables, the distribution of I can be accurately approximated with the so-called $\alpha - \mu$ distribution [79].

5.3.1. $\alpha - \mu$ approximation to the sum of i.i.d. $G - G$ variates

Let $I = \sum_{n=1}^{\mathbf{N}} I_n$ be a sum of $\mathbf{N}$ i.i.d. $G - G$ variates. We propose to approximate the PDF $f_I(I)$ and CDF $F_I(I)$ of I by the α-μ PDF and CDF given in [79]

$$f_I(I) = \frac{\alpha \mu^{\mu} I^{\alpha\mu - 1}}{\widehat{I}^{\alpha\mu}\Gamma(\mu)} \exp\left(-\mu \frac{I^{\alpha}}{\widehat{I}^{\alpha}}\right) \tag{28}$$

$$F_I(I) = 1 - \frac{\Gamma(\mu, \mu I^{\alpha}/\widehat{I}^{\alpha})}{\Gamma(\mu)} \tag{29}$$

In (28), (29), $\alpha, \mu > 0$ are the distribution parameters, $\widehat{I} = \mathbb{E}\{I^{\alpha}\}^{1/\alpha}$ is a scale parameter and $\Gamma(\cdot,\cdot)$ is the incomplete gamma function [28, Eq. (8.350/2)]. The motivation behind this approximation is twofold: First, in a recently published work [3] it was shown that the gamma distribution can be used to approximate the sum of independent $G - G$ variates. We feel that the use of a more generic distribution, which includes as special case the gamma distribution (in the α-μ case by setting $\alpha = 1$), will result in a more accurate approximation. Second, as it will become evident, the estimation of the parameters of the resulting α-μ PDF requires the knowledge of the first, the second and the fourth moment of I, which can be easily evaluated given the moments of I_n. Therefore, the resulting PDF incorporates information regarding the mean, the variance *and* the kurtosis of I. In order to render (28) and (29) an accurate approximation, moment-based estimators for α, μ and $\widehat{I}$ are used. These estimators are obtained as [79]

$$\frac{\Gamma^2(\mu + 1/\alpha)}{\Gamma(\mu)\Gamma(\mu + 2/\alpha) - \Gamma^2(\mu + 1/\alpha)} = \frac{\mathbb{E}^2\{I\}}{\mathbb{E}\{I^2\} - \mathbb{E}^2\{I\}} \tag{30}$$

$$\frac{\Gamma^2(\mu + 2/\alpha)}{\Gamma(\mu)\Gamma(\mu + 4/\alpha) - \Gamma^2(\mu + 2/\alpha)} = \frac{\mathbb{E}^2\{I^2\}}{\mathbb{E}\{I^4\} - \mathbb{E}^2\{I^2\}} \tag{31}$$

$$\widehat{I} = \frac{\mu^{\frac{1}{\alpha}}\Gamma(\mu)\mathbb{E}\{I\}}{\Gamma\left(\mu + \frac{1}{\alpha}\right)} \tag{32}$$

The required moments $\mathbb{E}\{I\}$, $\mathbb{E}\{I^2\}$ and $\mathbb{E}\{I^4\}$ can be evaluated using (13) and the multinomial identity as

$$\begin{aligned}\mathbb{E}\{I^{\nu}\} = \sum_{j_1=0}^{\nu} \sum_{j_2=0}^{j_1} \cdots \sum_{j_{\mathbf{N}-1}=0}^{j_{\mathbf{N}-2}} \binom{\nu}{j_1}\binom{j_1}{j_2}\cdots\binom{j_{\mathbf{N}-2}}{j_{\mathbf{N}-1}} \\ \times \mathbb{E}\{{I_1}^{\nu - j_1}\}\mathbb{E}\{{I_2}^{j_1 - j_2}\}\cdots\mathbb{E}\{{I_{\mathbf{N}}}^{j_{\mathbf{N}-1}}\}\end{aligned} \tag{33}$$

where ν is positive integer. Using Maple, the command lines given in (34), can be utilized to obtain α and μ in a computationally efficient manner. In this case, $In \triangleq \mathbb{E}\{I^n\}$, $n = 1, 2, 4$. The parameter $\widehat{I}$ can be finally obtained using (32). To demonstrate the accuracy of this

analysis, Fig. 5 shows the exact and approximate CDFs of the sum of two and nine i.i.d. G − G variates with $\overline{I} = 1$ for different values of parameters k and m. As it can be observed, in all considered test cases, the proposed approximation is highly accurate and practically indistinguishable from the exact CDF curves. A comparison of the proposed method with the one proposed in [3] reveals that our method performs equally well for both small and large values of **N**. Thus, a correcting factor, similar to the one introduced in [3] to obtain a sufficient approximation accuracy, is no longer required. Moreover, in [21], an approximate expression for the CDF of I in terms of Meijer-G functions [28, Eq. (9.301)] is provided. However, since the evaluation of Meijer-G functions can be sometimes laborious, (29) may be preferable to [21] in terms of computational complexity. Finally, our derived formulas are simpler than those presented in [14], since the latter are expressed as infinite series and require the computation of convolutional sums.

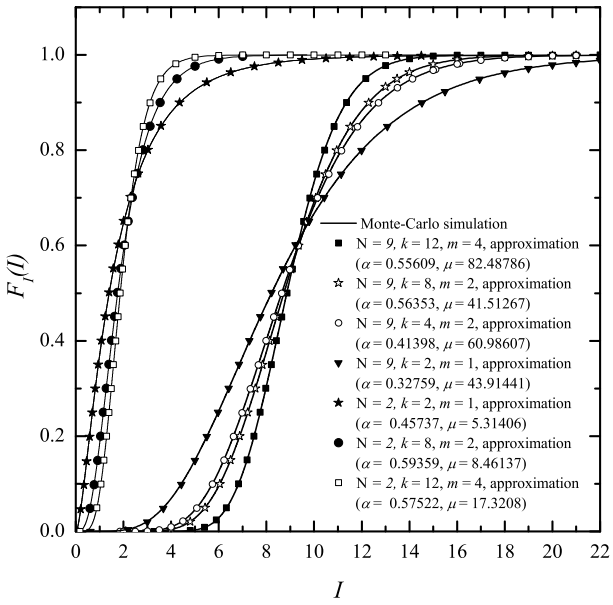

Figure 5. Exact and approximate CDF of the sum of $\mathbf{N} = 2$ and $\mathbf{N} = 9$ i.i.d G − G variates

In Fig. 6 the OP of the considered system is plotted as a function of the inverse normalized outage threshold $\overline{\mu}/\mu_{th}$ for $L = 2$km and $L = 4$km. The parameters k and m are obtained using (10) and (11) assuming $\lambda = 1550$nm, $C_n^2 = 1.7 \times 10^{-14}\text{m}^{-2/3}$ and $D/L \to 0$. Both numerically evaluated and computer simulation results are depicted. From the above mentioned plot, it is clear that the derived approximative expressions are highly accurate for every considered MIMO deployment and for all considered link distances.

To evaluate ABEP, the PDF of I, $f_I(I)$, at the combiner output, will be approximated by the PDF of a single channel given in (28) where the parameters α and μ are estimated as functions of k and m. Having obtained these parameters, the ABEP is easily obtained by substituting (28) into (21) and performing symbolic or numerical integration. In Fig. 7 the ABEP of the considered MIMO system is depicted as a function of the average electrical SNR, using the same parameters considered in the OP case. From the observation of Fig. 7, one can

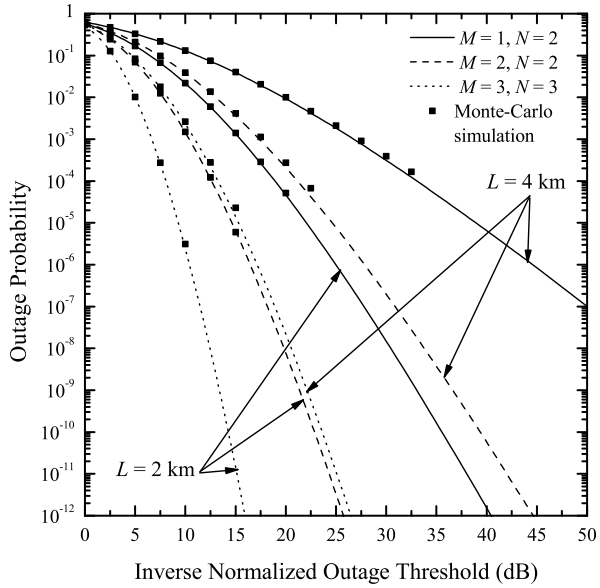

Figure 6. Outage Probability of MIMO FSO systems employing EGC and operating over i.i.d G − G fading channels as a function of the inverse normalized outage threshold, ($\lambda = 1550$nm, $C_n^2 = 1.7 \times 10^{-14}\text{m}^{-2/3}$ and $D/L \to 0$)

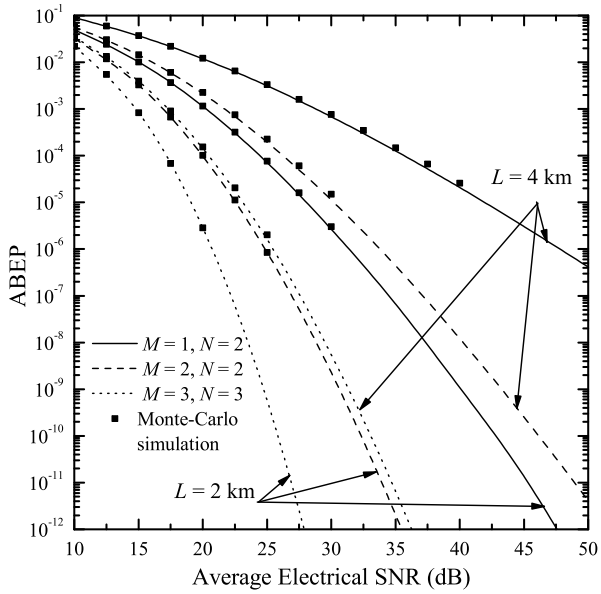

Figure 7. ABEP of MIMO FSO systems employing EGC and operating over i.i.d G − G fading channels as a function of the average electrical SNR, ($\lambda = 1550$nm, $C_n^2 = 1.7 \times 10^{-14}\text{m}^{-2/3}$ and $D/L \to 0$)

verify similar findings to that mentioned in Fig. 6 regarding the accuracy of the proposed approximation.

$$
\begin{aligned}
&\text{X1} := \text{I1\^{}2}/(\text{I2} - \text{I1\^{}2}); \text{X2} := \text{I2\^{}2}/(\text{I4} - \text{I2\^{}2});\\
&\text{f1} := \text{X1} - (\text{GAMMA}(\text{mu} + 1/\text{alpha}))\text{\^{}2}/(\text{GAMMA}(\text{mu}) * \text{GAMMA}(\text{mu} + 2/\text{alpha})\\
&- (\text{GAMMA}(\text{mu} + 1/\text{alpha}))\text{\^{}2}) = 0;\\
&\text{f2} := \text{X2} - (\text{GAMMA}(\text{mu} + 2/\text{alpha}))\text{\^{}2}/(\text{GAMMA}(\text{mu}) * \text{GAMMA}(\text{mu} + 4/\text{alpha})\\
&- (\text{GAMMA}(\text{mu} + 2/\text{alpha}))\text{\^{}2}) = 0;\\
&\text{SOL} := \text{fsolve}(\{\text{f1}, \text{f2}\}, \{\text{alpha}, \text{mu}\}, \{\text{alpha} = 0..1000, \text{mu} = 0..1000\});
\end{aligned}
\tag{34}
$$

6. Conclusions

In this chapter we presented a thorough performance analysis of FSO communication systems using spatial diversity over G − G distributed atmospheric turbulence channels. We obtained accurate approximated closed-form expressions and rapidly convergent infinite series representations for the average bit error probability and the outage probability of SIMO and MIMO FSO systems. Our results demonstrated that significant performance gains can be obtained when multiple apertures at the transmitter and/or receiver are used.

Acknowledgement

This work was partially supported by the Special Research Account of the National and Kapodistrian University of Athens.

Author details

Kostas Peppas
National Center For Scientific Research "Demokritos", Laboratory of Wireless Communications, Institute of Informatics and Telecommunications, 15310 Athens, Greece

Hector E. Nistazakis and George S. Tombras
Department of Electronics, Computers, Telecommunications and Control, Faculty of Physics, National and Kapodistrian University of Athens, 15784, Athens Greece

Vasiliki D. Assimakopoulos
Institute of Environmental Research and Sustainable Development of the National Observatory of Athens, I. Metaxa and Vas. Pavlou, Athens, 15236, Greece

7. References

[1] Aalo, V. A. [1995]. Performance of maximal-ratio diversity systems in a correlated Nakagami fading environment, *IEEE Trans. Commun.* 43: 2360–2369.

[2] Aalo, V. A. & Piboongungon, T. [2005]. On the multivariate generalized Gamma distribution with exponential correlation, *Proc. IEEE Global Telecommun. Conf. (GLOBECOM'05)*, Vol. 3, St. Louis, Missouri, USA.

[3] Al-Ahmadi, S. & Yanikomeroglu, H. [2010]. On the approximation of the generalized-K distribution by a gamma distribution for modeling composite fading channels, *IEEE Trans. Wireless Commun.* 9(2): 706–713.

[4] Al-Habash, M. A., Andrews, L. C. & Phillips, R. L. [2001]. Mathematical model for the irradiance pdf of a laser beam propagating through turbulent media, *Opt. Eng* 40(8): 1554–1562.
[5] Alexandropoulos, G. C., Sagias, N. C., Lazarakis, F. I. & Berberidis, K. [2009]. New results for the multivariate Nakagami-*m* fading model with arbitrary correlation matrix and applications, *IEEE Trans. Wireless Commun.* 8(1): 245–255.
[6] Andrews, L. [2004a]. Atmospheric optics, *SPIE Optical Engineering Press* .
[7] Andrews, L. [2004b]. Field guide to atmospheric optics, *SPIE Field Guides* FG02.
[8] Andrews, L., Al-Habash, M., Hopen, C. & Phillips, R. [2001]. Theory of optical scintillation: Gaussian beam wave model, *Waves in Random Media* 11: 271–291.
[9] Andrews, L. & Philips, R. [1985]. I-K distribution as a universal propagation model of laser beams in atmospheric turbulence, *Journal of the Optical Society of America A* 2(2): 160–163.
[10] Andrews, L. & Philips, R. [1986]. Mathematical genesis of the I-K distribution for random optical fields, *Journal of the Optical Society of America A* 3(11): 1912–1919.
[11] Andrews, L., Phillips, R. & Hopen, C. [2001]. Laser beam scintillation with applications, *SPIE Optical Engineering Press* .
[12] Arnon, S. [2003]. *Optical wireless communications*, Encyclopedia of Optical Engineering, New York: Marcel Dekker, pp. 1866–1886.
[13] Assimakopoulos, D., Lalas, D., Helmis, C. & Caroubalos, C. [1980]. An atmospheric turbulence probe, *IEEE Transactions on Geoscience and Remote Sensing* GE18: 347–353.
[14] Bayaki, E., Schober, R. & Mallik, R. [2009]. Performance analysis of MIMO free-space optical systems in gamma-gamma fading, *IEEE Trans. Commun.* 57(11): 3415–3424.
[15] Bithas, P. S., Sagias, N. C. & Mathiopoulos, P. T. [2009]. The bivariate generalized-K distribution and its application to diversity receivers, *IEEE Trans. Commun.* 57(9): 2655–2662.
[16] Bithas, P. S., Sagias, N. C., Mathiopoulos, P. T., Karagiannidis, G. K. & Rontogiannis, A. A. [2006]. On the performance analysis of digital communications over generalized-K fading channels, *IEEE Commun. Lett.* 10(5): 353–355.
[17] Bloom, S. [2001]. The physics of free-space optics, *AirFiber, Inc.* 2003.
[18] Bradley, E. & Antonia, R. [1979]. Structure parameters in the atmospheric surface layer, *Quarterly Journal of the Royal Meteorological Society* 105(445): 695–705.
[19] Castillo-Vazquez, C., Garcia-Zambrana, A. & Castillo-Vazquez, B. [2009]. Closed-form BER expression for FSO links with transmit laser selection over exponential atmospheric turbulence channels, *Electr. Lett.* 23(45).
[20] Caughey, S. & Palmer, S. [1979]. Some aspects of turbulence structure through the depth of the convective boundary layer, *Quarterly Journal of the Royal Meteorological Society* 105(446): 811–827.
[21] Chatzidiamantis, N. & Karagiannidis, G. [2011]. On the distribution of the sum of gamma-gamma variates and applications in RF and optical wireless communications, *IEEE Trans. Commun.* 59(5): 1298–1308.
[22] Chiani, M., Dardari, D. & Simon, M. K. [2003]. New exponential bounds and approximations for the computation of error probability in fading channels, *IEEE Trans. Wireless Commun.* 2: 840–845.
[23] Churnside, J. & Clifford, S. [1987]. Log-normal ricean probability density function of optical scintillations in the turbulent atmosphere, *Journal of the Optical Society of America A* 4(10): 1923–1930.

[24] Filho, F. C. M., Jayasuriya, D., Cole, R., Helmis, C. & Assimakopoulos, D. [1988]. Correlated humidity and temperature measurements in the urban atmospheric boundary layer, *Meteorol. Atmos. Phys.* 39: 197–202.
[25] Gagliardi, R. & Karp, S. [1995]. *Optical Communications*, John Wiley, New York.
[26] Garcia-Zambrana, A. [2007]. Error rate performance for STBC in free-space optical communications through strong atmospheric turbulence, *IEEE Commun. Lett.* 11(5): 390–392.
[27] Garcia-Zambrana, A., Castillo-Vazquez, C., Castillo-Vazquez, B. & Hiniesta-Gomez, A. [2009]. Selection transmit diversity for FSO links over strong atmospheric turbulence channels, *IEEE Photonics Technol. Lett.* 21(14): 1017–1019.
[28] Gradshteyn, I. & Ryzhik, I. M. [2000]. *Tables of Integrals, Series, and Products*, 6 edn, Academic Press, New York.
[29] Haas, S. M. & Shapiro, J. H. [2003]. Capacity of wireless optical communications, *IEEE J. Select. Areas Commun.* 21(8): 1346–1357.
[30] Henniger, H. & Wilfert, O. [2010]. An introduction to free-space optical communications, *Radioengineering* 19(2): 203–212.
[31] Ishimaru, A. [1978]. Wave propagation and scattering in random media, *Academic Press* 2.
[32] Kamalakis, T., Sphicopoulos, T., Muhammad, S. & Leitgeb, E. [2006]. Estimation of the power scintillation probability density function in free-space optical links by use of multicanonical monte carlo sampling, *Optics Letters* 31(21): 3077–3079.
[33] Karagiannidis, G. K., Zogas, D. A. & Kotsopoulos, S. A. [2003]. On the multivariate Nakagami-*m* distribution with exponential correlation, *IEEE Trans. Commun.* 51(8): 1240–1244.
[34] Karp, S., Gagliardi, R. M., Moran, S. E. & Stotts, L. [1988]. *Optical channels: fibers, clouds, water and the atmosphere*, New York: Plenum Press.
[35] Katsis, A., Nistazakis, H. E. & Tombras, G. S. [2009]. Bayesian and frequentist estimation of the performance of free space optical channels under weak turbulence conditions, *Journal of the Franklin Institute* 346: 315–327.
[36] Keddar, D. & Arnon, S. [2004]. Urban optical wireless communication networks: the main challenges and possible solutions, *IEEE Opt. Commun.* 42(5): 51–57.
[37] Kunkel, K. & Walters, D. [1982]. Intermittent turbulence in measurements of the temperature structure parameter under very stable conditions, *Boundary-layer meteorology* 22(1): 49–60.
[38] Laourine, A., Stephenne, A. & Affes, S. [2007]. Estimating the ergodic capacity of log-normal channels, *IEEE Communications Letters* 11(7): 568–570.
[39] Lawrence, R. & Strohben, J. [1970]. A survey of clear air propagation effects relevant to optical communications, *Proceedings of the IEEE* 58: 1523–1545.
[40] Lombardo, P. & Farina, A. [1996]. Coherent radar detection against K-distributed clutter with partially correlated texture, *Signal Process.* 48: 1–15.
[41] MacGovern, A., Nahrstedt, D. & Johnson, M. [2000]. Atmospheric propagation for tactical directed energy applications, *Proceedings SPIE* 4034: 128–139.
[42] Majumdar, A. [1984a]. Higher-order statistics of laser irradiance fluctuations due to turbulence, *Journal of the Optical Society of America* 1: 1067–1074.
[43] Majumdar, A. [1984b]. Uniqueness of statistics derived from moments of irradiance fluctuations in atmospheric optical propagation, *Optics Communications* 50(1): 1–7.

[44] Majumdar, A. K. [2005]. Free-space laser communication performance in the atmospheric channel, *J. Opt. Fiber Commun. Rep.* 2: 345–396.
[45] Mallik, R. K. [2003]. On multivariate Rayleigh and exponentials distributions, *IEEE Trans. Inf. Theory* 49(6): 1499–1515.
[46] Navidpour, S. M., Uysal, M. & Kavehrad, M. [2007]. Performance of free-space optical transmission with spatial diversity, *IEEE Trans. Wireless Commun.* 6(8): 2813–2819.
[47] Nistazakis, H., Assimakopoulos, V. & Tombras, G. [2011]. Performance estimation of free space optical links over negative exponential atmospheric turbulence channels, *Optik* 122(24): 2191–2194.
[48] Nistazakis, H. E. [in press, 2012]. A time-diversity scheme for wireless optical links over exponentially modeled turbulence channels, *OPTIK* .
[49] Nistazakis, H. E. & Tombras, G. [in press, 2012]. On the use of wavelength and time diversity in optical wireless communication systems over gamma-gamma turbulence channels, *Journal of Optics and Laser Technology* .
[50] Nistazakis, H. E., Tsiftsis, T. A. & Tombras, G. S. [2009]. Performance analysis of free space optical communication systems over atmospheric turbulence channels, *IET Communications* 3(8): 1402–1409.
[51] Nistazakis, H., Karagianni, E., Tsigopoulos, A., Fafalios, M. & Tombras, G. [2009]. Average capacity of optical wireless communication systems over atmospheric turbulence channels, *J. Lightw. Technol* 27(8): 974–979.
[52] Nistazakis, H., Katsis, A. & Tombras, G. [2012]. *On the Reliability and Performance of FSO and Hybrid FSO Communication Systems over Turbulent Channels*, Nova Publishers, Turbulence: Theory, Types and Simulation.
[53] Nistazakis, H., Tsigopoulos, A., Hanias, M., Psychogios, C., Marinos, D., Aidinis, C. & Tombras, G. [2011]. Estimation of outage capacity for free space optical links over I-K and K turbulent channels, *Radioengineering* 20(2): 493–498.
[54] Niu, M., Cheng, J. & Holzman, J. F. [2010]. Exact error rate analysis of equal gain and selection diversity for coherent free-space optical systems on strong turbulence channels, *Optics Express* 18(13): 13915–13926.
[55] Peppas, K. [2011]. A simple, accurate approximation to the sum of gamma-gamma variates and applications in MIMO free-space optical systems, *IEEE Photon. Technol. Lett.* 23(13): 839–841.
[56] Peppas, K. P., Alexsandropoulos, G. C., Datsikas, C. K. & Lazarakis, F. I. [2011]. Multivariate gamma-gamma distribution with exponential correlation and its applications in radio frequency and optical wireless communictions, *IET Antennas and Propag.* 5: 364–371.
[57] Peppas, K. P. & Datsikas, C. K. [2010]. Average symbol error probability of general-order rectangular quadrature amplitude modulation of optical wireless communication systems over atmospheric turbulence channels, *J. Opt. Commun. Netw.* 2(2): 102–110.
[58] Peppas, K. & Sagias, N. C. [2009]. A trivariate Nakagami-*m* distribution with arbitrary covariance matrix and applications to generalized selection diversity receivers, *IEEE Trans. Commun.* 57(7): 1896–1902.
[59] Popoola, W., Ghassemlooy, Z., Lee, C. & Boucouvalas, A. [2010]. Scintillation effect on intensity modulated laser communication systems - laboratory demonstration, *Optics and Laser Technology* 42: 682–692.
[60] Prudnikov, A. P., Brychkov, Y. A. & Marichev, O. I. [1986]. *Integrals and Series Volume 3: More Special Functions*, 1 edn, Gordon and Breach Science Publishers.

[61] Rachmani, R. & Arnon, S. [2010]. Wavelength diversity in turbulence channels for sensor networks, *IEEE 26th Convention of Electrical and Electronics Engineers in Israel, IEEEI* pp. 915–918.
[62] Razavi, M. & Shapiro, J. [2005]. Wireless optical communications via diversity reception and optical preamplification, *IEEE Trans. Wireless Commun.* 4: 975–983.
[63] Safari, M. & Uysal, M. [2008]. Do we really need space-time coding for free-space optical communication with direct detection, *IEEE Trans. Wireless Commun.* 7(11): 4445–4448.
[64] Sagias, N. C. & Karagiannidis, G. K. [2005]. Gaussian class multivariate Weibull distributions: Theory and applications in fading channels, *IEEE Trans. Inf. Theory* 51(10): 3608–3619.
[65] Sandalidis, H. G. & Tsiftsis, T. A. [2008]. Outage probability and ergodic capacity of free-space optical links over strong turbulence, *Electronics Letters* 44(1): 46–47.
[66] Sandalidis, H. G., Tsiftsis, T. A., Karagiannidis, G. K. & Uysal, M. [2008]. BER performance of FSO links over strong atmospheric turbulence channels with pointing errors, *IEEE Commun. Lett.* 12(1): 44–46.
[67] Sim, C. H. [1993]. Generation of poisson and gamma random vectors with given marginals and covariance matrix, *Journal of Statistical Computation and Simulation* 47(1): 1–10.
[68] Simon, M. K. & Alouini, M. S. [2005]. *Digital Communication over Fading Channels*, 2 edn, Wiley, New York.
[69] Tsiftsis, T. A., Sandalidis, H. G., Karagiannidis, G. K. & Uysal, M. [2009]. Optical wireless links with spatial diversity over strong atmospheric turbulence channels, *IEEE Trans. Wireless Commun.* 8(2): 951–957.
[70] Uysal, M., Navidpour, S. M. & Li, J. [2004]. Error rate performance of coded free-space optical links over strong turbulence channels, *IEEE Commun. Lett.* 8(10): 635–637.
[71] Vetelino, F., Young, S. & Andrews, L. [2007]. Fade statistics and aperture averaging for gaussian beam waves in moderate to strong turbulence, *Applied Optics* 46(18): 3780–3789.
[72] Wainright, E., Refai, H. H. & Jr., J. J. S. [2005]. Wavelength diversity in free-space optics to alleviate fog effects, *Proceedings of SPIE* 5712(16): 110–118.
[73] Wang, Z., Zhong, W.-D., Fu, S. & Lin, C. [2009]. Performance comparison of different modulation formats over free-space optical (FSO) turbulence links with space diversity reception technique, *IEEE Photnics Journal* 1(6): 277–285.
[74] Wilson, S. G., Brandt-Pearce, M., Cao, Q. & Baedke, M. [2005]. Optical repetition MIMO transmission with multipulse PPM, *IEEE J. Sel. Areas Commun.* 23: 1901–1910.
[75] Wilson, S. G., Brandt-Pearce, M., Cao, Q. & Leveque, J. H. [2005]. Free-space optical MIMO transmission with Q-ary PPM, *IEEE Trans. Commun.* 53(8): 1402–1412.
[76] Wyngaard, J. [1992]. Atmospheric turbulence, annual review of fluid mechanics, *Annual Review of Fluid Mechanics* 24: 205–234.
[77] Wyngaard, J., Izumi, Y. & Jr., S. C. [1971]. Behavior of the refractive-index-structure parameter near the ground, *Journal of the Optical Society of America A* 61(12): 1646–1650.
[78] Xu, F., Khalighi, A., Causse, P. & Bourennane, S. [2009]. Channel coding and time-diversity for optical wireless links, *Optics Express* 17(2): 872–887.
[79] Yacoub, M. D. [2007]. The α-μ distribution: A physical fading model for the Stacy distribution, *IEEE Trans. Veh. Technol.* 56(1): 27–34.
[80] Z. Wang, W.-D. Zhong, S. F. & Lin, C. [2009]. Performance comparison of different modulation formats over free-space optical (fso) turbulence links with space diversity reception technique, *IEEE Photonics Journal* 1(6): 277–285.

[81] Zhu, X. & Kahn, J. M. [2002]. Free-space optical communications through atmospheric turbulence channels, *IEEE Transaction on Communications* 50(8): 1293–1300.

[82] Zhu, X. & Kahn, J. M. [2003a]. Markov chain model in maximum-likelihood sequence detection for free-space optical communication through atmospheric turbulence channels, *IEEE Trans. Commun.* 51(3): 509–516.

[83] Zhu, X. & Kahn, J. M. [2003b]. Performance bounds for coded free-space optical communications through atmospheric turbulence channels, *IEEE Trans. Commun.* 51(8): 1233–1239.

[84] Zhu, X., Kahn, J. M. & Jin, W. [2003]. Mitigation of turbulence-induced scintillation noise in free-space optical links using temporal-domain detection techniques, *IEEE Photon. Technol. Lett.* 15(4): 623–625.